Macromolecular Bioscience
www.mbs-journal.de

Magnetic Levitational Assembly of Differentiated SH-SY5Y Cells for Aβ-Induced 3D Alzheimer's Disease Modeling and Curcumin Screening

*Rumeysa Bilginer-Kartal and Ahu Arslan-Yildiz**

Alzheimer's disease is one of the prevalent neurodegenerative diseases and is characterized by amyloid beta aggregate (Aβ) accumulation. This study reports an Aβ 1–42 induced 3D Alzheimer's disease modeling utilizing differentiated SH-SY5Y spheroids, which is carried out by Magnetic levitation approach, and the neuroprotective effect of Curcumin is further investigated on this model. For this purpose, SH-SY5Y spheroids are differentiated using Retinoic acid-Brain-derived neurotrophic factor sequentially during 3D cell culture. Differentiated spheroids maintained high viability and exhibited significant neuronal characteristics, as evidenced by increasing β-III tubulin and NeuN expressions. 3D Alzheimer's disease model formation and neurotoxicity of Aβ 1–42 aggregates are investigated on un-/differentiated spheroids, resulting in 65% and 51% cell viability, respectively. Characterization of the 3D Alzheimer's disease model is done by immunostaining of Choline acetyltransferase to investigate cholinergic neuron activity loss, showing a 2.2 decrease in fluorescence intensity. Further, Curcumin treatment on the 3D Alzheimer's disease model resulted in augmenting cell viability, confirming neuroprotective effect of Curcumin on Aβ 1–42 induced Alzheimer's disease model. This study highlighted the magnetic levitation-based fabrication of Aβ 1-42-induced 3D Alzheimer's disease model successfully, offering a promising experimental platform for other neurodegenerative disease research and potential clinical applications.

1. Introduction

Alzheimer's disease is one of the most common neurodegenerative diseases, affecting more than 50 million people around the world.[1–4] The main hallmark of Alzheimer's disease is the accumulation of amyloid beta (Aβ) aggregates outside the cell, which is an initiation factor starting neurodegeneration.[5–7] The development of new and effective drugs against Alzheimer's disease is extremely important. Although many drugs have been tried in clinical studies for Alzheimer's disease so far, the failure rate has been recorded as 99.6% mostly due to inadequacies of conventional 2D in vitro and animal models.[8–10] Despite their contributions, these experimental models struggle to recapitulate key aspects of Alzheimer's disease pathology due to failure in mimicking human physiology, therefore more realistic experimental platforms are required.[11–13]

Recently, 3D modeling of Alzheimer's disease has accelerated due to all these problems. Alzheimer's disease has been modeled with different 3D cell culture methods, mostly conducting scaffold-based approaches, and the Matrigel matrix was widely used as a scaffold in these examples.[5,14–20] Despite the significant contribution of these approaches in modeling Alzheimer's disease, Matrigel-based scaffolds have challenges in mimicking the mechanical, chemical, and biological properties of the human brain tissue microenvironment and extracellular matrix due to its origin, as well as heterogeneity, and batch-to-batch variability.[21] Furthermore, concerns about the potential cytotoxicity of scaffolds and their uncontrolled degradation profiles are additional drawbacks of the scaffold-based approaches.[22,23] Besides, the organoid model approach has been utilized in modeling Alzheimer's disease.[24–27] These miniaturized and simplified versions of organs have the potential to replicate many aspects of brain structure and function. Despite their promise, this approach faces significant limitations due to low reproducibility, labor-intensive procedures, extremely high cost, and ethical concerns.[28] Therefore, scaffold-free approaches emerged as a powerful strategy to overcome all these drawbacks. These approaches eliminate the need for external scaffolding materials and allow cells to self-organize, leading to spheroid formation. Among these, Magnetic levitation (MagLev) technology is one of the scaffold-free approaches that recently gained attention due

R. Bilginer-Kartal, A. Arslan-Yildiz
Department of Bioengineering
Izmir Institute of Technology (IZTECH)
Izmir 35430, Turkey
E-mail: ahuarslan@iyte.edu.tr

The ORCID identification number(s) for the author(s) of this article can be found under https://doi.org/10.1002/mabi.202400658

DOI: 10.1002/mabi.202400658

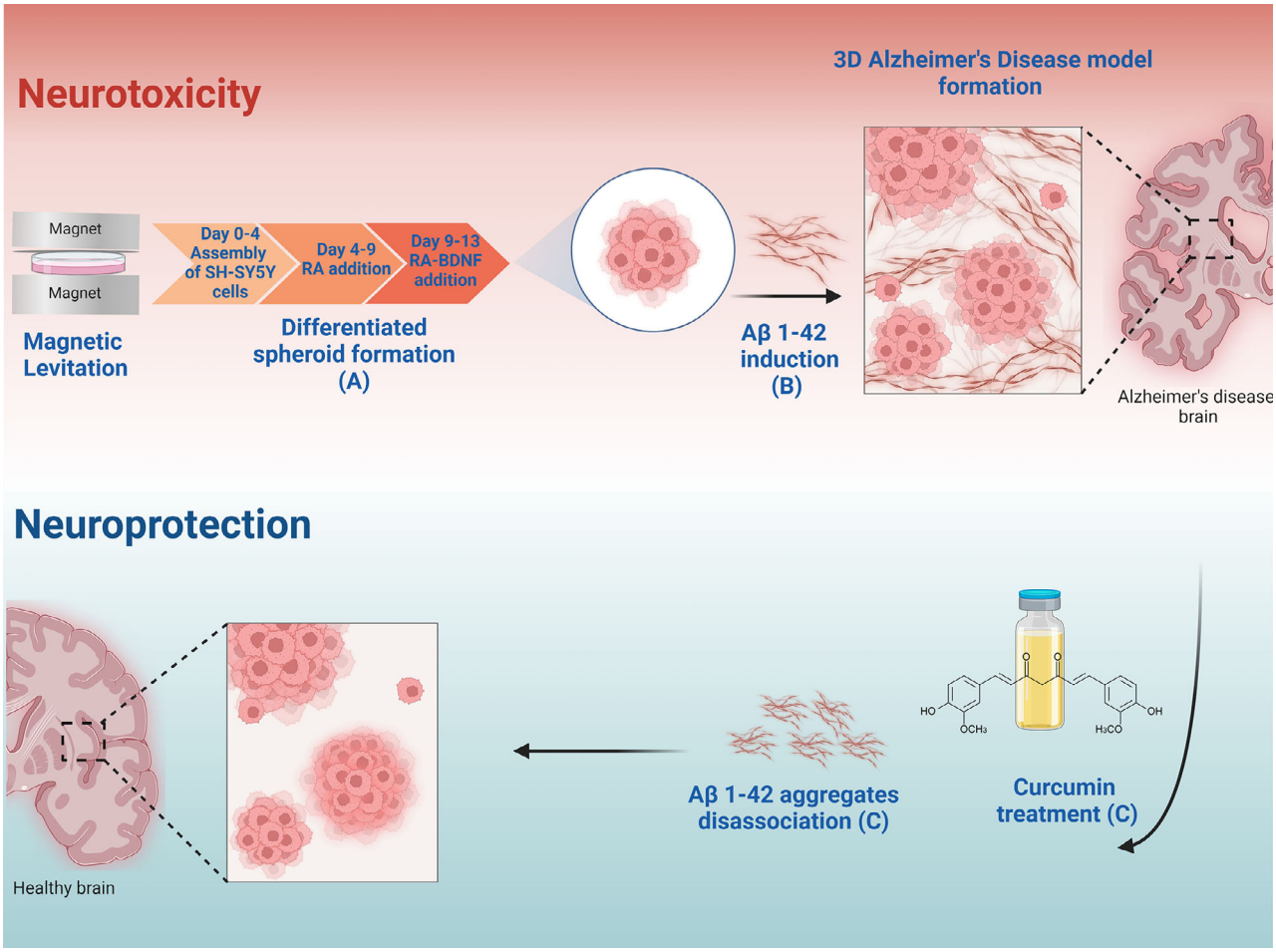

Figure 1. Depiction of the Aβ-induced 3D Alzheimer's disease model formation; A) differentiated SH-SY5Y spheroid formation *via* MagLev B) Introducing Aβ 1–42 aggregates into 3D cell culture C) Curcumin treatment and disassociation of Aβ 1–42 aggregates. (*The illustration was created by BioRender.com*).

to its rapid, easy operation and process.[29–31] Also, MagLev technology provides high reproducibility and cost-effective biofabrication without any ethical concerns.[32] MagLev technology, with its numerous advantages over other 3D fabrication methods, stands out as a promising tool in this field.

In recent years, MagLev technology has been utilized extensively for 3D cell culture formation, with innovative studies demonstrating its effectiveness.[33–39] The MagLev system operates on the principle of suspending objects at a certain levitation height by balancing the forces acting on the objects in the magnetic field.[33] This facilitates the formation of 3D spheroid structures through enhanced cell-cell interactions by employing contactless manipulation.[34] This method also allows precise control over spheroid size and area by adjusting various parameters while ensuring high cell viability even in long-term cultures.[35] The utilization of MagLev technology in 3D Alzheimer's disease modeling has not been explored in existing studies, indicating a significant gap within this field.

The primary objective of this study is to develop an Aβ 1-42-induced 3D Alzheimer's disease model using differentiated SH-SY5Y spheroids, conducted through the MagLev approach (**Figure 1**). Additionally, the study explores the neuroprotective effects of Curcumin on the fabricated 3D Alzheimer's disease model, known for its ability to disassociate Aβ 1–42 aggregates.[40,41] For this purpose, SH-SY5Y cells, a human neuroblastoma cell line, were cultured in the MagLev setup. Gadobutrol (Gx) was utilized as a paramagnetic agent, thereby magnetizing the cell culture medium and promoting the formation of spheroids. SH-SY5Y spheroids were differentiated during 3D cell culture using Retinoic acid (RA) and Brain-derived neurotrophic factor (BDNF), which plays a crucial role in promoting neuronal differentiation (Figure 1A). Characterization of the spheroids involved measuring cell viability (%) and area versus circularity analysis. Cell viability for un-/differentiated spheroids was evaluated *via* Live-Dead assay. Before modeling 3D Alzheimer's disease, the formation of Aβ 1–42 aggregates was confirmed using Congo red assay and Scanning Electron Microscopy (SEM) analyses. Subsequently, Aβ 1–42 aggregates were introduced to the 3D cell culture environment to form Aβ –induced 3D Alzheimer's disease model (Figure 1B). The developed 3D Alzheimer's disease model was characterized and confirmed by immunostaining Choline acetyltransferase (ChAT) to examine the loss of cholinergic neuron activity. Next, the disassociation potential of Curcumin on Aβ 1–42 aggregates was evaluated using Congo red and Thioflavin T assays exogenously. Then, Curcumin was applied to a 3D Alzheimer's disease model to

investigate its neuroprotective effect (Figure 1C). Results showed that Curcumin disassociated Aβ 1–42 aggregates into smaller fragments and protected cells against Aβ-induced neurotoxicity while augmenting cell viability. As a result, the formation of an Aβ-induced 3D Alzheimer's disease model via MagLev methodology was successfully shown. Overall, this approach provides an experimental platform that offers new avenues to model other neurodegenerative diseases and test therapeutic candidates.

2. Results and Discussion

2.1. Optimization of Experimental Parameters

The developed MagLev setup was designed to provide easy and rapid formation of SH-SY5Y spheroids utilizing the MagLev principle.[35] Gx concentration and cell number were optimized for 24h (Figures S1 and S2, Supporting Information). Cells started to gather with the help of magnetic, gravitational, and buoyancy forces, and cell clusters were observed starting from the 4th h. Compact spheroid formation was observed at the end of 24h even at low Gx concentrations (Figure S1A, Supporting Information), which is attributed to cell-cell interaction through magnetic guidance, leading to the formation of 3D cellular clusters, eventually spheroids.[35] Furthermore, SH-SY5Y spheroids demonstrated remarkable cell viability in all concentrations, ranging between 98–96% (Figure S1B, Supporting Information). Next, cell number optimization was carried out at 10 mM Gx which provides high cell viability, as well as sufficient levitation of cells (Figure S2, Supporting Information). When 5×10^3 cells were cultured, smaller spheroids were formed within 24h and irregular and larger cellular clusters were formed when 1×10^5 cells were cultured (Figure S2A, Supporting Information). Moreover, high cell viability was observed for varied cell numbers, ranging between 100–94% (Figure S2B, Supporting Information) Although there was a non-significant difference between 25×10^3 and 50×10^3 in terms of cell viability and morphological structure, subsequent culturing studies were conducted using 25×10^3 cell numbers since lower cell number provides a more controlled environment and spheroid formation parameters can be tuned in this way.[35]

2.2. Differentiation of SH-SY5Y Cells During 3D Cell Culture in MagLev Setup

Cells reflecting mature neuron-like phenotype or behavior are pivotal in nervous system-related studies, especially for neurodegenerative diseases, including Alzheimer's disease.[42] SH-SY5Y cells can possess similar properties with primary neurons after sequential differentiation via RA-BDNF[43–47] Neuronal cells in 2D cell culture cannot maintain primary neuron features,[48] therefore, in this study, SH-SY5Y cells were cultured in 3D and differentiated using RA-BDNF, (**Figure 2**).[47,49]

Differentiation of SH-SY5Y cells in 3D cell culture was maintained using 10 mM Gx for the long-term, and spheroid features were evaluated by means of structure and viability (Figure 2). It was observed that 10 mM Gx was successfully paramagnetized cell culture environment and sufficient enough for levitation of spheroids for 9 days, which is consistent with the literature.[34,35] Besides this concentration provided high cell viability as shown in fluorescence microscopy images (Figure 2A); ranging between 94–95% for undifferentiated, and 98–100% for differentiated spheroids (Figure 2B,C). The higher viability of differentiated spheroids can be attributed to as activation of the Phosphoinositide 3-kinase/Protein kinase B pathway, which involves cell survival induced by BDNF.[50] Here, the differentiation process was successfully conducted in parallel with 3D spheroid formation inside the MagLev setup. On the other hand, cells individually differentiated in 2D and then cultured in the MagLev setup formed smaller cell clusters with low cell viability rather than 3D spheroids (Figure S3, Supporting Information).

In addition, bright-field images showed that un-/differentiated spheroids preserved their circular and compact structures, while differentiated spheroids exhibited more compact structures compared to undifferentiated ones (Figure 2A). This can be explained by higher levels of cell adhesion molecules in differentiated SH-SY5Y spheroids compared to undifferentiated ones.[51] Circularity and area analysis were done to characterize the structural features of un-/differentiated SH-SY5Y spheroids, which were influenced by varied factors such as Gx concentration, cell number, and incubation time.[35] The circularity of un-/differentiated reached 0.87 and 0.89 on day 9, respectively. Besides, the spheroid area increased in undifferentiated spheroids, while differentiated spheroids remained more compact for 9 days, ranging between 0.162–0.224 mm^2 and 0.09–0.107 mm^2, respectively (Figure 2D,E). This might originate from RA treatment, which leads to p21 activation,[44,52] resulting in the inhibition of cell proliferation due to arrest in the G1/S phase of the cell cycle.[52]

Overall, the findings highlighted that differentiation of cells in MagLev results in proper spheroid size with remarkable cell viability, indicating the suitability of the MagLev system for potential use in 3D neuronal differentiation.

Immunostaining provides an additional method for assessing cellular differentiation through the expression of neuronal markers. Differentiated neuron cells exhibit significant differences in the secretion of some neuronal markers β-III Tubulin is a neuron-specific class of tubulin that increases with the rate of neuronal differentiation[53] and Neuronal nuclei (NeuN) is localized in the nucleus, and it is observed when cells become postmitotic.[54,55] **Figure 3** shows fluorescence images of β-III Tubulin and NeuN immunostaining, along with fluorescence intensity analysis for un-/differentiated SH-SY5Y spheroids. The highest β-III Tubulin expression was seen in differentiated groups on day 9[44] (Figure 3A–C) and 6.8, 1.5, and 2.3-fold fluorescence intensity increase was observed between un-/differentiated spheroids on days 5,7, and 9, respectively (Figure 3D). On the other hand, NeuN was slightly expressed in undifferentiated spheroids, while it was significantly expressed in differentiated groups (Figure 3A–E). These findings affirm that differentiated 3D spheroids maintained neuronal features, which is consistent with the literature.[44,47,51,56]

2.3. Alzheimer's Disease Modeling in 3D

Aβ 1–40 and/or Aβ 1–42 peptides are commonly encountered in Alzheimer's pathology, and they have been utilized as tools for Alzheimer's disease modeling.[57–61] However, Aβ 1–42 is

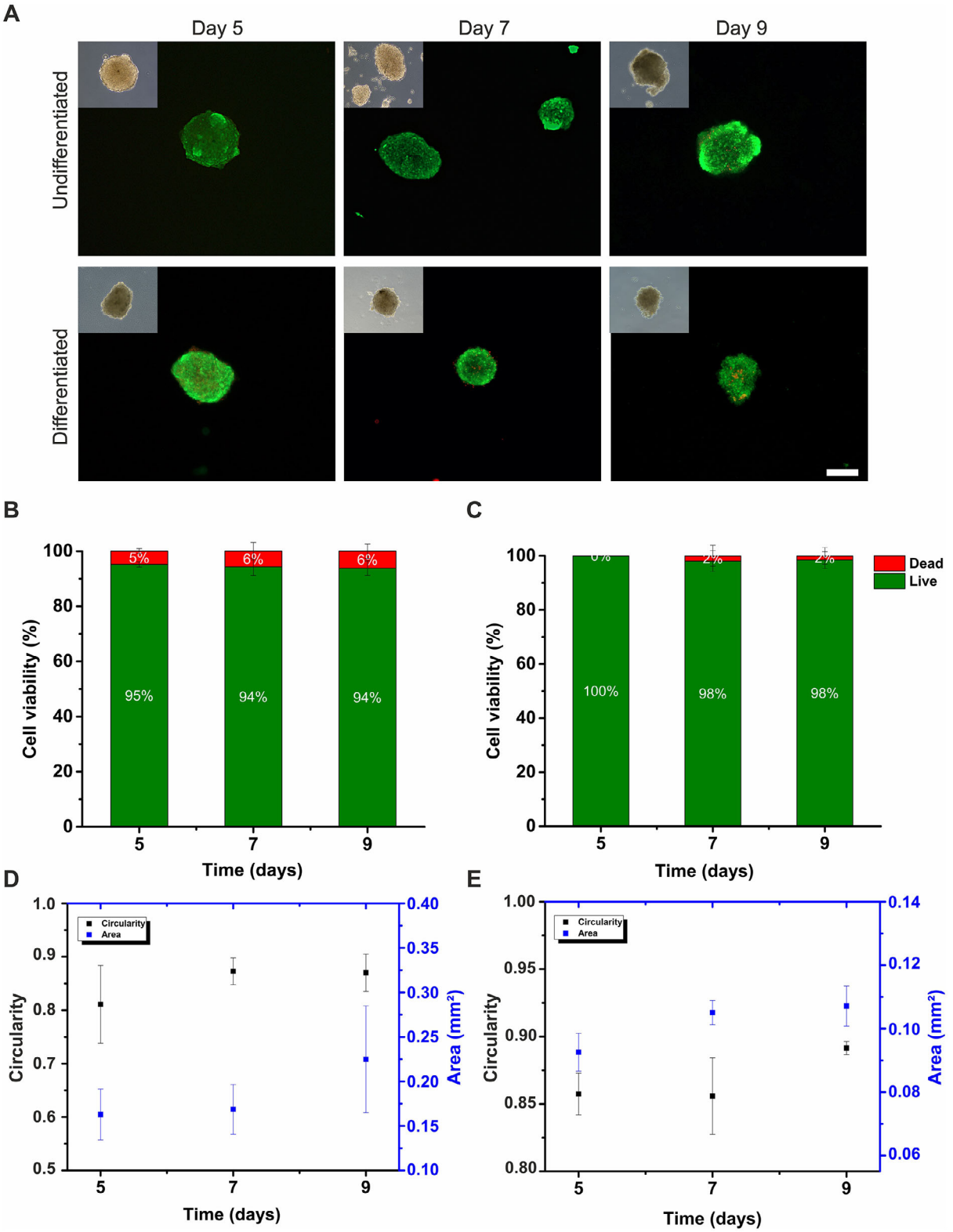

Figure 2. Bright-field and fluorescence microscopy images for un-/differentiated spheroids analyzed by Live-Dead assay. *Scale bar:200 μm*. (**Green**: Live, **Red**: Dead). Cell viability results of B) Undifferentiated and C) Differentiated spheroids. Circularity and area analysis of D) Undifferentiated and E) Differentiated spheroids on days 5,7, and 9.

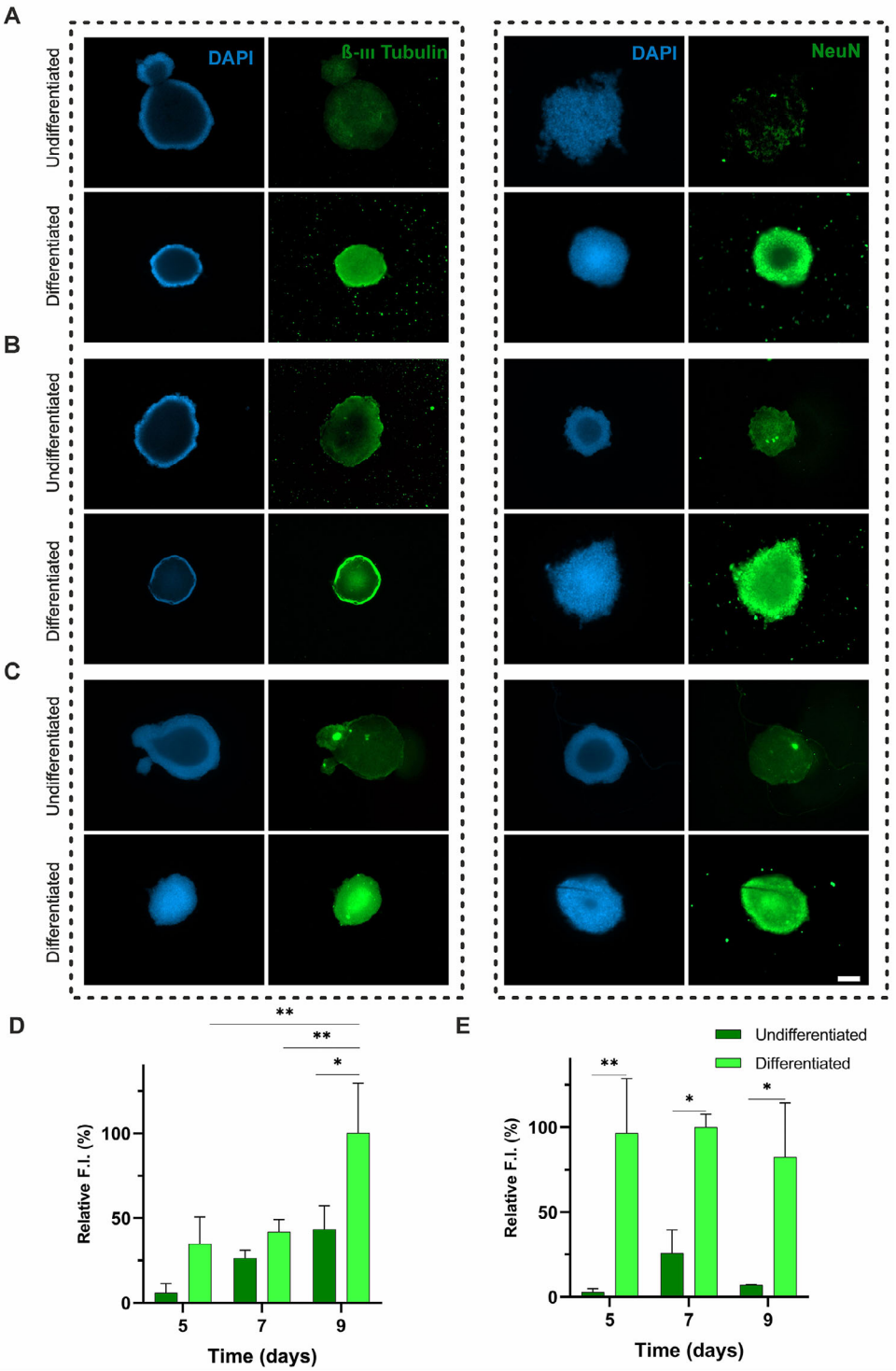

Figure 3. Fluorescence microscopy images of β-III tubulin and NeuN for un-/differentiated SH-SY5Y spheroids on A) day 5 B) day 7 and C) day 9 (**Blue**: DAPI, **Green**: β-III tubulin and NeuN). (*Scale bar:* 100 µm). Relative fluorescence intensity (F.I.) of D) β-III tubulin and e) NeuN ($n = 3$, $^{*}p < 0.05$, $^{**}p < 0.01$).

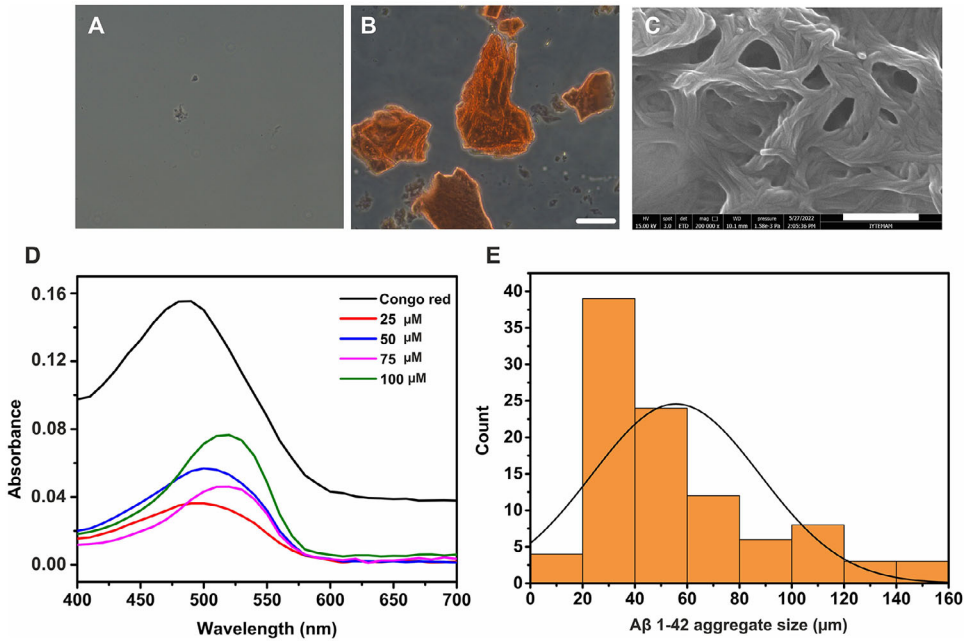

Figure 4. Bright-field microscopy images of Aβ 1–42 after applying Congo red staining; A) monomer and B) aggregate. (*Scale bar*: 50 μm), C) SEM image of Aβ 1–42 aggregates (*Scale bar*: 500 nm). D) Spectrophotometric analysis of Aβ 1–42 aggregates (25–100 μM) by Congo red staining, E) Size distribution profile of Aβ 1–42 aggregates (n) = 100.

insoluble, prone to aggregate formation, and more toxic than Aβ 1–40[62,63] thus, Aβ 1–42 has been frequently employed in modeling Alzheimer's disease.[57,58,64,65] Therefore, here Aβ 1–42 was used to model Alzheimer's disease. Prior to 3D Alzheimer's disease modeling, aggregate formation was confirmed by Congo red staining[66] and SEM analysis (**Figure 4**). Congo red staining result of Aβ 1–42 monomer and aggregates were given in Figure 4A,B, respectively. Aβ 1–42 aggregates were stained with Congo red to confirm the aggregate formation, while monomers were not stained (Figure 4A,B). Additionally, Aβ 1–42 aggregate formation was also observed by SEM analysis as depicted in Figure 4C. Besides, the interaction of Aβ 1–42 aggregate and Congo red dye was investigated by spectrophotometric analysis.[67] The absorbance maximum of Congo red dye was observed at 490 nm, which shifted to 540 nm after complex formation, as expected[67] (Figure 4D). After confirming aggregate formation, the size distribution profile of Aβ 1–42 aggregate was obtained via light microscopy images, predominantly ranging between 20–60 μm (Figure 4E). It overlaps with the literature where Aβ aggregate size was reported as 40–80 μm for 3D in vitro and 20–60 μm for post-mortem brain slices.[64,68]

Aβ 1–42 aggregates are key for Alzheimer's disease pathology by triggering neurotoxicity,[69] therefore, this study investigated the neurotoxicity of Aβ 1–42 aggregates on SH-SY5Yspheroids. For this purpose, spheroids were exposed to 10–50 μM Aβ 1–42 aggregates to determine neurotoxic parameters reducing cell viability to ≈50%.[57,60] A concentration-dependent decrease in cell viability was observed, with significant cell death at 50 μM for un-/differentiated spheroids[70] (Figure S4A, Supporting Information). Cell viability of undifferentiated spheroids decreased to 71% while it decreased to 68% in differentiated spheroids with a significant difference (p <0.05) (**Figure 5**A). Furthermore, the neurotoxic effect of 50 μM Aβ 1–42 for long-term was investigated on un-/differentiated spheroids to model 3D Alzheimer's disease.

Next, the neurotoxicity of 50 μM Aβ 1–42 aggregates was investigated based on incubation time. Increased cell death was observed in correlation with the extended incubation time of Aβ 1–42 aggregates (Figure S4B, Supporting Information). Cell viability decreased to 65% for undifferentiated spheroids, while it decreased to 51% for differentiated spheroids on day 7 (Figure 5B). It has been reported in the literature that Aβ 1–42 aggregates reduce cell viability to ≈50% and below for modeling Alzheimer's disease, thus the expected neurotoxicity was observed in differentiated spheroids.[57,60] Also, there is a significant difference in cell viability between un-/differentiated spheroids on day 7. This indicates that differentiated spheroids are more vulnerable to neurotoxins compared to undifferentiated spheroids, which is consistent with similar studies.[44,71,72] This can be attributed to undifferentiated cells having smaller surface areas due to lacking longer neurites, resulting in smaller contact areas with Aβ 1–42 aggregates.[72] The findings support that differentiated spheroids in 3D are a more suitable experimental model for studying Alzheimer's disease.[72] Besides, ChAT expression has been investigated in Alzheimer's disease models for cholinergic neuron activity loss.[73–75] The characterization of the 3D Alzheimer's disease model was carried out by immunostaining of ChAT biomarker (Figure 5C,D). Fluorescence microscopy images and F.I. calculations show that ChAT expression notably reduced (2.2-fold) in the 3D Alzheimer's disease model compared to the control group (Figure 5C,D), which correlates with the literature.[76]

Overall, these findings indicate that the 3D Alzheimer's disease model was successfully developed, offering a valuable

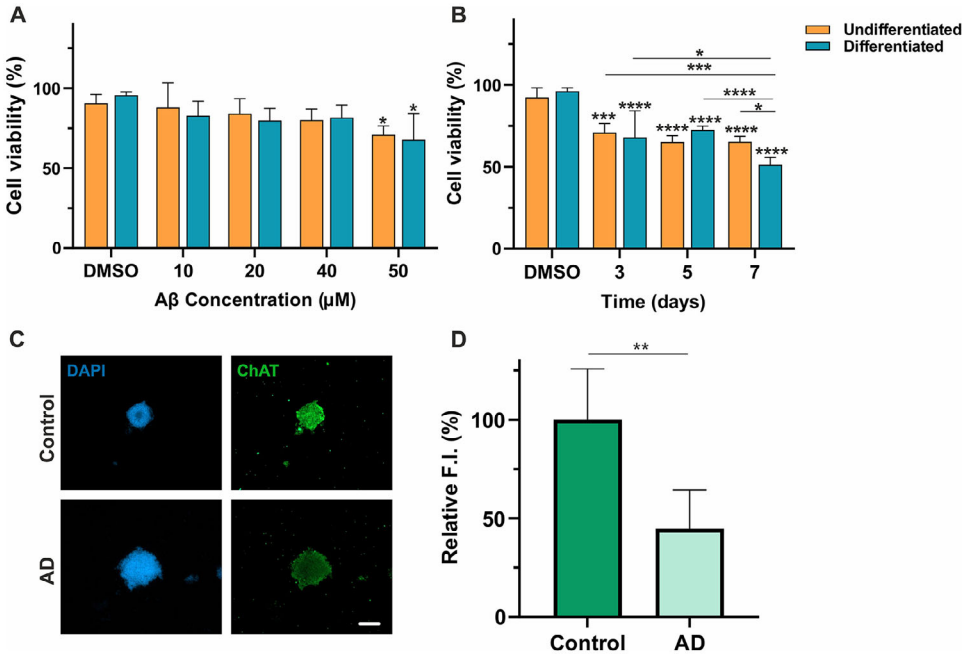

Figure 5. Neurotoxicity screening of Aβ 1–42 on SH-SY5Y spheroids; cell viability results for A) 3 days, 10–50 μM, and B) 3–7 days, 50 μM Aβ 1–42 exposure, ($n = 5$, $^{*}p < 0.05$, $^{**}p < 0.01$, $^{***}p < 0.001$, $^{****}p < 0.0001$, *compared to DMSO control of each group* via *two-way ANOVA followed by Tukey's test*) C) Fluorescence microscopy images of ChAT biomarker (*Scale bar*:200 μm) and D) Calculated fluorescence intensity (F.I.) of ChAT biomarker for Control and AD (Alzheimer's disease) model via Image J analysis.(**Blue**: DAPI, **Green**: ChAT ($n = 4$, $^{**}p < 0.01$).

tool for studying Alzheimer's disease and testing potential therapeutic candidates. Hence, differentiated spheroids were utilized for 3D Alzheimer's disease modeling and investigating the neuroprotective effect of Curcumin in further studies.

2.4. Investigating the Neuroprotective Effect of Curcumin

Curcumin has the potential as a neuroprotective agent in Alzheimer's disease by disassociating Aβ aggregates and reducing neurotoxicity.[59,77,78] Therefore, Curcumin can be an alternative compound to suppress Alzheimer's disease progression.[59] For this purpose, Curcumin was incubated with 1–42 aggregates exogenously to evaluate its effect on their disassociation. The samples were monitored by bright-field microscopy and also analyzed by Congo red and Thioflavin T assays[79–83] (**Figure 6**). Bright-field images show that Curcumin effectively disassociated Aβ 1–42 aggregates and reduced their size with increasing Curcumin concentration (Figure 6A). In addition, the aggregate size of Aβ 1–42 was measured after applying Curcumin (Figures S5A and S5E, Supporting Information), where the average Aβ 1–42 aggregate size decreased from 55.69 to 37.83 μm. Besides, Curcumin's capability in disassociating Aβ 1–42 aggregates was analyzed quantitatively by Congo red and Thioflavin T assays.[84] Relative absorbance and fluorescence intensity (F.I.) decreased following Curcumin treatment, ranging between 58-38% and 71-53%, respectively with significant differences (Figure 6B,C). These results confirmed that Curcumin possesses the ability to disassociate Aβ 1–42 aggregates by disrupting intra- and interstrand distances of preformed fibrils, as reported in studies.[85]

Later, the evaluation of the neuroprotective effect of Curcumin was investigated on differentiated SH-SY5Y spheroids. Fluorescence microscopy images showed that Curcumin decreased Aβ-induced cell death owing to its neuroprotective effect and high cell viability was observed in spheroids treated with Curcumin (Figure S6, Supporting Information). Curcumin increased cell viability within the given concentration range, and especially 25 μM prevented Aβ-induced neurotoxicity, augmenting cell viability from 51% to 94% with a significant difference (**Figure** 7A). In addition, the disassociation of Aβ 1–42 aggregates on 3D spheroids was investigated by immunostaining of Aβ 1–42 before and after Curcumin treatment (Figure 7B). Fluorescence microscopy images showed that Curcumin successfully disassociated Aβ 1–42 into smaller fragments, as expected.[85,86] Overall, these findings indicate that Curcumin has neuroprotective properties against Aβ aggregates, suppressing Aβ aggregate accumulation and preventing Aβ-induced cell death in 3D Alzheimer's disease supported by the literature.[69,86–88]

3. Conclusion

This study reported the formation of a 3D Alzheimer's disease model using an Aβ-induced approach and investigation of the neuroprotective effect of Curcumin. MagLev technology was employed to fabricate SH-SY5Y spheroids for 3D Alzheimer's disease modeling and SH-SY5Y spheroids were differentiated using RA-BDNF sequentially for 9 days during 3D cell culture. For this purpose, cell number and paramagnetic agent (Gx) concentration were optimized before differentiation and fabricated un-/differentiated spheroids exhibited remarkable cell viability above 90%. Following differentiation, neuronal characterization

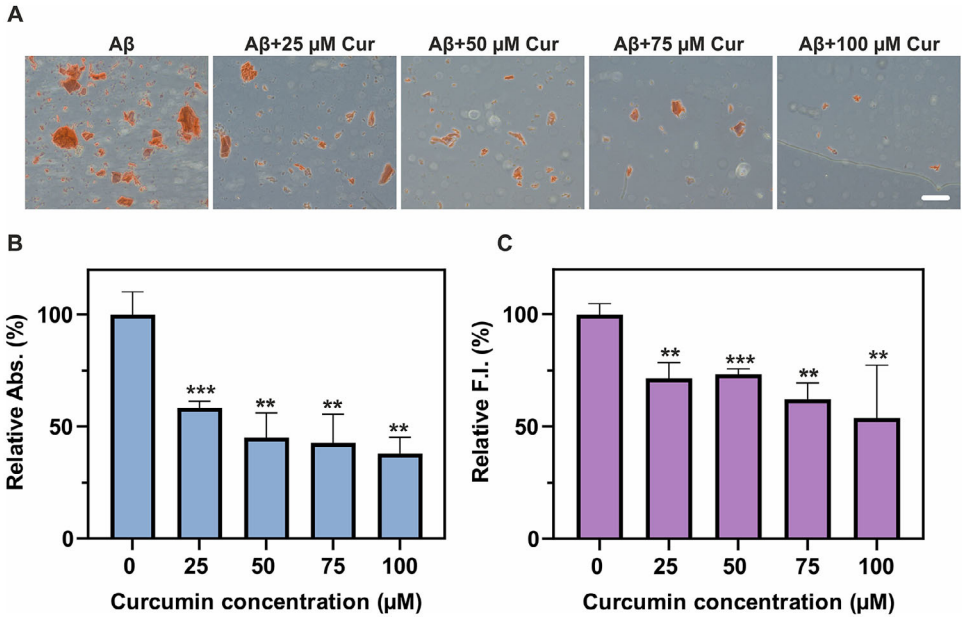

Figure 6. Curcumin effect on disassociation of Aβ 1–42 aggregates; A) Bright-field microscopy images of Aβ 1–42 aggregates (*Scale bar:* 200 μm), B) Congo red assay results displaying relative absorbance (Abs.), and C) Thioflavin T assay results displaying relative fluorescence intensity (F.I.), following Curcumin treatment for 72h ($n = 6$, $^{**}p < 0.01$ $^{***}p < 0.001$ *compared Aβ group* (0 μM) via *one-way ANOVA followed by Tukey's test*).

was carried out by immunostaining of β-III tubulin and NeuN. Differentiated groups significantly expressed β-III tubulin and NeuN compared to undifferentiated spheroids on day 9. Before 3D Alzheimer's disease modeling, Aβ 1–42 aggregates were characterized using bright-field microscopy, SEM, and Congo red assay, confirming successful aggregate formation.

Neurotoxicity of Aβ 1–42 aggregates on un-/differentiated SH-SY5Y spheroids was evaluated at different concentrations and incubation times; where 50 μM Aβ 1–42 aggregate resulted in 65% cell viability for undifferentiated and 51% cell viability for differentiated spheroids for 7 days incubation. Next, 3D Alzheimer's disease model formation was characterized by evaluating the cholinergic activity loss via immunostaining of ChAT, resulting in a 2.2-fold decrease in F.I. for the 3D Alzheimer's disease model compared to the control. A decrease in cell viability and cholinergic activity confirms the formation of 3D Alzheimer's disease model successfully Next, the potential of Curcumin to disassociate Aβ 1–42 aggregates was investigated by Congo red and Thioflavin T assays exogenously. Concentration dependent-absorbance and F.I. decrease showed that Curcumin disassociated Aβ 1–42 aggregate into smaller fragments. When Curcumin was applied to the Aβ-induced 3D Alzheimer's disease model, cell viability increased from 51% to 94%, indicating that Curcumin suppressed the neurotoxicity of Aβ 1–42 aggregates. This result was supported by immunostaining of Aβ 1–42 aggregates on 3D spheroids, resulting in smaller Aβ 1–42 aggregate fragments following Curcumin treatment. Overall, these findings highlighted the neuroprotective potential of Curcumin against Aβ aggregates, representing a significant step forward in Alzheimer's disease research. In conclusion, it revealed that the 3D Alzheimer's disease model was successfully developed through differentiation of SH-SY5Y cells during 3D cell culture

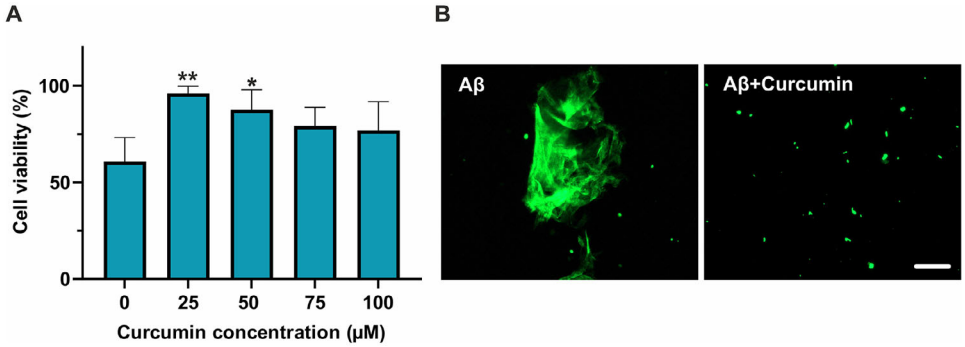

Figure 7. Investigating neuroprotective effect of Curcumin on Aβ 1–42 aggregates in 3D spheroids; A) Cell viability after Curcumin treatment for Aβ–induced 3D Alzheimer's disease model, B) Fluorescence microscopy images of Aβ 1–42 aggregates on 3D spheroids before and after Curcumin treatment (*Scale bar:* 100 μm) ($n = 5$, $^{*}p < 0.05$, $^{**}p < 0.01$ compared 0 μM *via one-way ANOVA followed by Tukey's test*).

in MagLev setup offering a valuable tool for understanding the pathophysiology of Alzheimer's disease, as well as other neurodegenerative diseases, and testing the potential therapeutic agents.

4. Experimental Section

Standard 2D Cell Culture: SH-SY5Y (Human bone marrow neuroblastoma, ATCC® CRL-2266™) was used in the study;[89] in literature, it is the most commonly used cell line in Alzheimer's disease modeling studies.[57,59,60,72,75] The cells were cultured in a standard medium, containing DMEM (Gibco), 15% FBS (Gibco), 1% PenStrep at 37 °C, and 5% CO_2 conditions. The harvested cells were used for further studies.

Formation of SH-SY5Y Spheroids via MagLev: 3D cell culture of SH-SY5Y cells was carried out using a MagLev setup, as depicted elsewhere.[35] In brief, the setup comprises two permanent NdFeB N35 disc magnets arranged in an anti-Helmholtz configuration and integrated into poly (methyl methacrylate) (PMMA) holders. A Petri dish (Ibidi-80131) containing cells, cell medium, and the paramagnetic agent, Gadobutrol (Gx; Gadovist, Bayer) was placed inside the setup between the magnets for 3D cell culturing. Then, the MagLev setup was kept in the incubator at 37 °C, 5% CO_2 conditions for spheroid formation.

The optimal Gx concentration and cell number were determined for 3D cell culture formation. First, 10–100 mM Gx was investigated at 25 × 10^3 cell number, then cell number optimization was conducted at 10 mM Gx for 5–100 × 10^3 cells. Following the optimization of Gx concentration and cell number, sequential differentiation of SH-SY5Y spheroids was also done inside the MagLev setup via RA (Retinoic acid) and BDNF (Brain-derived neurotrophic factor) addition as described elsewhere.[47] Briefly, 10 µM RA was supplemented to cell culture after obtaining SH-SY5Y spheroids. This step was repeated on the 3rd day of cell culture followed by the addition of 50 ng mL^{-1} BDNF along with RA on the 5th day and repeated every two days until the 9th day.

Characterization of SH-SY5Y Spheroids: Following spheroid formation, structural changes of un-/differentiated spheroids were monitored by light microscopy, while cell viability was assessed by Live-Dead,[90] (ATT Bioquest) for 9 days. % cell viability and circularity versus area changes were characterized using Image J software (NIH). Neuronal characterization was done by immunostaining of β-III tubulin and NeuN on days 5, 7, and 9, and quantified by F.I. analysis using Image J software.

3D Alzheimer's Disease Modeling Through Aβ 1–42 Induction: Aβ 1–42 aggregates were utilized on SH-SY5Y spheroids to obtain an Aβ 1–42 induced 3D Alzheimer's disease model. Therefore, Aβ 1–42 aggregates were generated by dissolving monomers (Royobiotech) in DMSO and incubated at 37 °C for 72h. Congo red staining was used to confirm aggregate formation by light microscopy monitoring and spectral analysis. For this, 40 µM CR was added to 0–100 µM Aβ 1–42 aggregates and incubated overnight. The spectrum of Congo red (Isolab) was recorded between 400–700 nm[79] using a Multiskan™ GO microplate spectrophotometer (Thermo Fischer Scientific). Next, aggregates were monitored by light microscopy and the formation of Aβ 1–42 aggregates was assessed by SEM analysis. Furthermore, Aβ 1-42-induced Alzheimer's disease formation in 3D was performed by adding 10–50 µM Aβ 1–42 aggregates to un-/differentiated spheroids on days 3, 5 and 7. For this purpose produced 3D spheroids were transferred out of the MagLev setup and Aβ 1–42 aggregates were introduced directly to spheroids in a cell culture medium without Gx. Later, the neurotoxicity profile and cell viability were analyzed through Live-Dead[91] images for modeling Alzheimer's disease. Cell viability (%) was evaluated using Image J software.

Characterization of the 3D Alzheimer's disease model was carried out by immunostaining of ChAT (ABClonal) to examine cholinergic neuron activity[73–75,92] In addition, to monitor Aβ 1–42 aggregates un-/differentiated spheroids were immunostained with anti-Aβ (Proteintech) and visualized by fluorescence microscopy. F.I. of ChAT and Aβ 1–42 aggregates were quantified using Image J software for both un-/differentiated spheroids.

Investigating the Neuroprotective Effect of Curcumin: The effect of Curcumin in dissociating Aβ 1–42 aggregates was assessed through Congo red and Thioflavin T assay before cell culture studies. For this purpose, 25, 50, 75, and 100 µM Curcumin (AFG Bioscience) was incubated with 50 µM Aβ 1–42 aggregates for 72h. Congo red and Thioflavin T assays were carried out separately using a spectrophotometer.[93,94] Curcumin cytotoxicity between 25–100 µM was evaluated on both un-/differentiated spheroids then, it was introduced to spheroids, along with 50 µM Aβ 1–42 aggregates. After 72h incubation, a Live-Dead assay was carried out to assess cell viability, and cell viability (%) was evaluated using Image J software.

Statistical Analysis: Each experiment was conducted using at least three independent replicates, with data presented as mean ± SD. Statistical analysis was performed using GraphPad Prism 9 software (GraphPad Prism, Inc., San Diego, USA), employing one-way and two-way ANOVA followed by Tukey's test for multiple comparisons. Statistical significance between groups was determined as follows: $^{*}p \leq 0.05$, $^{**}p \leq 0.01$, $^{***}p \leq 0.001$, $^{****}p \leq 0.0001$.

Supporting Information

Supporting Information is available from the Wiley Online Library or from the author.

Acknowledgements

The authors acknowledge İzmir Institute of Technology Biotechnology and Bioengineering Research and Application Center. The authors would like to thank Prof. Dr. Pınar Akan for the fruitful discussion on the development of the Alzheimer's disease model. Rumeysa Bilginer-Kartal gratefully acknowledges the Scientific and Technological Research Council of Turkey (TUBITAK) 2211-A National Graduate Scholarship program. This study has been supported by the Turkish Academy of Sciences (TÜBA), in the framework of the Young Scientist Award Program (TÜBA-GEBİP/2019) and IZTECH-Scientific Research Project (IYTE BAP Grant no: 2022IYTE-1-0058).

Conflict of Interest

The authors declare no conflict of interest.

Author Contributions

R.B.-K. was responsible for the investigation, methodology, and writing of the original draft, while A.A.-Y. contributed to the conceptualization, supervision, and review & editing of the writing.

Data Availability Statement

The data that support the findings of this study are available from the corresponding author upon reasonable request.

Keywords

3D Alzheimer's disease model, Aβ 1–42 aggregates, Curcumin screening, differentiated SH-SY5Y spheroids, magnetic levitation

Received: December 30, 2024
Revised: March 4, 2025
Published online: March 25, 2025

[1] A. P. Porsteinsson, R. S. Isaacson, S. Knox, M. N. Sabbagh, I. Rubino, *J. Prev. Alzheimers Dis.* **2021**, *8*, 371.
[2] L. Lai, C. Zhao, M. Su, X. Li, X. Liu, H. Jiang, C. Amatore, X. Wang, *Biomater. Sci.* **2016**, *4*, 1085.
[3] N. Rouleau, W. L. Cantley, V. Liaudanskaya, A. Berk, C. Du, W. Rusk, E. Peirent, C. Koester, T. J.-F. Nieland, D. L. Kaplan, *Macromol. Biosci.* **2020**, *20*, 2000004.
[4] S. De Sio, J. Waegele, T. Bhatia, B. Voigt, H. Lilie, M. Ott, *Macromol. Biosci.* **2023**, *23*, 2200527.
[5] V. D. Ranjan, L. Qiu, J. W.-L. Lee, X. Chen, S. E. Jang, C. Chai, K.-L. Lim, E.-K. Tan, Y. Zhang, W. M. Huang, L. Zeng, *Biomater. Sci.* **2020**, *8*, 4861.
[6] C. Qian, C. Yuan, C. Li, H. Liu, X. Wang, *Biomater. Sci.* **2020**, *8*, 5538.
[7] Y. Mitsuishi, M. Nakano, H. Kojima, T. Okabe, M. Nishimura, *ACS Chem. Neurosci.* **2024**, *15*, 1234.
[8] J. L. Cummings, T. Morstorf, K. Zhong, *Alzheimers Res. Ther.* **2014**, *6*, 37.
[9] J. Cummings, G. Lee, A. Ritter, K. Zhong, *Transl. Res. and Clinical Interventions* **2018**, *4*, 195.
[10] J. J. Sabbagh, J. W. Kinney, J. L. Cummings, *Neurobiol. Aging* **2013**, *34*, 169.
[11] C. D'Avanzo, J. Aronson, Y. H. Kim, S. H. Choi, R. E. Tanzi, D. Y. Kim, *BioEssays* **2015**, *37*, 1139.
[12] G. Cenini, M. Hebisch, V. Iefremova, L. J. Flitsch, Y. Breitkreuz, R. E. Tanzi, D. Y. Kim, M. Peitz, O. Brüstle, *Mol. Cell. Neurosci.* **2021**, *110*, 103568.
[13] S. H. Choi, Y. H. Kim, L. Quinti, R. E. Tanzi, D. Y. Kim, *Mol. Neurodegener* **2016**, *11*, 75.
[14] S. H. Choi, Y. H. Kim, M. Hebisch, C. Sliwinski, S. Lee, C. D'Avanzo, H. Chen, B. Hooli, C. Asselin, J. Muffat, J. B. Klee, C. Zhang, B. J. Wainger, M. Peitz, D. M. Kovacs, C. J. Woolf, S. L. Wagner, R. E. Tanzi, D. Y. Kim, *Nature* **2014**, *515*, 274.
[15] S. Lomoio, R. S. Pandey, N. Rouleau, B. Menicacci, W. Kim, W. L. Cantley, P. G. Haydon, D. A. Bennett, T. L. Young-Pearse, G. W. Carter, D. L. Kaplan, G. Tesco, *Mol. Psychiatry* **2023**, *28*, 5390.
[16] C. Cuní-López, R. Stewart, L. E. Oikari, T. H. Nguyen, T. L. Roberts, Y. Sun, C. C. Guo, M. K. Lupton, A. R. White, H. Quek, *J. Neuroinflammation* **2024**, *21*, 50.
[17] M. A. Hernández-Sapiéns, E. E. Reza-Zaldívar, R. R. Cevallos, A. L. Márquez-Aguirre, K. Gazarian, A. A. Canales-Aguirre, *Front Cell Neurosci* **2020**, *14*, 151.
[18] Y. Zhang, H. Chen, X. Long, T. Xu, *Bioact. Mater.* **2022**, *11*, 192.
[19] C. Benwood, J. Walters-Shumka, K. Scheck, S. M. Willerth, *Bioelectron Med.* **2023**, *9*, 10.
[20] Y. Shin, S. H. Choi, E. Kim, E. Bylykbashi, J. A. Kim, S. Chung, D. Y. Kim, R. D. Kamm, R. E. Tanzi, *Adv. Sci.* **2019**, *6*, 1900962.
[21] M. Hebisch, S. Klostermeier, K. Wolf, A. R. Boccaccini, S. E. Wolf, R. E. Tanzi, D. Y. Kim, *Adv. Sci.* **2023**, *10*, 2205037.
[22] Z. Zhou, W. Feng, B. K. Moghadas, N. Baneshi, B. Noshadi, S. Baghaei, D. A. Dehkordi, *Tissue Cell* **2024**, *88*, 102390.
[23] A. Louit, T. Galbraith, F. Berthod, *Bioengineering* **2023**, *10*, 93.
[24] X. Chen, G. Sun, E. Tian, M. Zhang, H. Davtyan, T. G. Beach, E. M. Reiman, M. Blurton-Jones, D. M. Holtzman, Y. Shi, *Adv. Sci.* **2021**, *8*, 2101462.
[25] S. Huang, Z. Zhang, J. Cao, Y. Yu, G. Pei, *Signal Transduction Targeted Ther.* **2022**, *7*, 176.
[26] S. S. Lavekar, J. Harkin, M. Hernandez, C. Gomes, S. Patil, K. C. Huang, S. S. Puntambekar, B. T. Lamb, J. S. Meyer, *Sci. Rep.* **2023**, *13*, 13827.
[27] W. Fan, C. Xudong, S. Yizheng, S. Wu, H. Wang, S. Suresh, S. Krishnan, M. Ramalingam, J. Deng, *J. Biomater. Tissue Eng.* **2022**, *12*, 888.
[28] A. Slanzi, G. Iannoto, B. Rossi, E. Zenaro, G. Constantin, *Front Cell Dev. Biol.* **2020**, *8*, 328.
[29] Q.-H. Gao, B. Wen, Y. Kang, W.-M. Zhang, *Biosens. Bioelectron.* **2022**, *204*, 114052.
[30] E. Quagliarini, L. Digiacomo, D. Caputo, A. Coppola, H. Amenitsch, G. Caracciolo, D. Pozzi, *Nanomaterials* **2022**, *12*, 1397.
[31] A. A. Ashkarran, T. Olfatbakhsh, M. Ramezankhani, R. C. Crist, W. H. Berrettini, A. S. Milani, S. Pakpour, M. Mahmoudi, *Adv. Healthcare Mater.* **2020**, *9*, 1901608.
[32] A. A. Ashkarran, M. Mahmoudi, *Trends Biotechnol.* **2021**, *39*, 311.
[33] E. Turker, A. Arslan-Yildiz, *ACS Biomater. Sci. Eng.* **2018**, *4*, 787.
[34] E. Türker, N. Demirçak, A. Arslan-Yildiz, *Biomater. Sci.* **2018**, *6*, 1745.
[35] R. Onbas, A. A Yildiz, *ACS Appl. Bio Mater.* **2021**, *4*, 1794.
[36] V. A. Parfenov, E. V. Koudan, E. A. Bulanova, P. A. Karalkin, F. DAS Pereira, N. E. Norkin, A. D. Knyazeva, A. A. Gryadunova, O. F. Petrov, M. M. Vasiliev, M. I. Myasnikov, V. P. Chernikov, V. A. Kasyanov, A. Y. Marchenkov, K. Brakke, Y. D. Khesuani, U. Demirci, V. A. Mironov, *Biofabrication* **2018**, *10*, 034104.
[37] W. L. Haisler, D. M. Timm, J. A. Gage, H. Tseng, T. C. Killian, G. R. Souza, *Nat. Protoc.* **2013**, *8*, 1940.
[38] G. R. Souza, J. R. Molina, R. M. Raphael, M. G. Ozawa, D. J. Stark, C. S. Levin, L. F. Bronk, J. S. Ananta, J. Mandelin, M.-M. Georgescu, *Nat. Nanotechnol.* **2010**, *5*, 291.
[39] Q.-H. Gao, W.-M. Zhang, H.-X. Zou, W.-B. Li, H. Yan, Z.-K. Peng, G. Meng, *Mater. Horiz.* **2019**, *6*, 1359.
[40] A. S. Darvesh, R. T. Carroll, A. Bishayee, N. A. Novotny, W. J. Geldenhuys, C. J. Van der Schyf, *Expert Opin Investig Drugs* **2012**, *21*, 1123.
[41] S. D. Voulgaropoulou, T. A. M. J. van Amelsvoort, J. Prickaerts, C. Vingerhoets, *Brain Res.* **2019**, *1725*, 146476.
[42] L. Agholme, T. Lindström, K. Kgedal, J. Marcusson, M. Hallbeck, *J. Alzheimer's Dis.* **2010**, *20*, 1069.
[43] I. Tonazzini, A. Cecchini, Y. Elgersma, M. Cecchini, *Adv. Healthcare Mater.* **2014**, *3*, 581.
[44] R. F. Simões, R. Ferrão, M. R. Silva, S. L. C. Pinho, L. Ferreira, P. J. Oliveira, T. Cunha-Oliveira, *Food Chem. Toxicol.* **2021**, *149*, 111967.
[45] M. Encinas, M. Iglesias, Y. Liu, H. Wang, A. Muhaisen, V. Ceña, C. Gallego, J. X. Comella, *J. Neurochem.* **2000**, *75*, 991.
[46] M. Şahin, G. Öncü, M. A. Yılmaz, D. Özkan, H. Saybaşılı, *Neurosci. Lett.* **2021**, *745*, 135628.
[47] R. Bilginer Kartal, A. A Yildiz, *ACS Omega* **2024**, *9*, 14955.
[48] D. H. Park, M. T. He, E. J. Cho, K. Morten, J. S. Go, *Biomed. Microdevices* **2023**, *25*, 22.
[49] K. R. Ko, N. W. Tam, A. G. Teixeira, J. P. Frampton, *Biotechnol. Prog.* **2020**, *36*, e2942.
[50] M. Encinas, M. Iglesias, N. Llecha, J. X. Comella, *J. Neurochem.* **1999**, *73*, 1409.
[51] G. S. Jung, K. M. Lee, J. K. Park, S. K. Choi, W. B. Jeon, *BMB Rep.* **2013**, *46*, 276.
[52] J. Qiao, P. Paul, S. Lee, L. Qiao, E. Josifi, J. R. Tiao, D. H. Chung, *Biochem. Biophys. Res. Commun.* **2012**, *424*, 421.
[53] N. Mundhara, D. Panda, *Mol. Cell. Biochem.* **2023**, *478*, 1961.
[54] Mullen R. J., Buck C. R., Smith A. M., *Development* **1992**, *116*, 201.
[55] M. G. dos Santos, J. R. Gomes, M. D. M. Costa, *Cell Biol. Int.* **2023**, *47*, 1883.
[56] B. S. Serdar, T. Erkmen, B. U. Ergür, P. Akan, S. Koçtürk, *Neurosci. Neurophysiol.* **2020**, *37*, 82.
[57] O. G. Calan, P. Akan, A. Cataler, C. Dogan, S. Kocturk, *Neurochem. Res.* **2016**, *41*, 1700.
[58] J. Park, B. K. Lee, G. S. Jeong, J. K. Hyun, C. J. Lee, S.-H. Lee, *Lab Chip* **2015**, *15*, 141.
[59] A. S. Abdul Manap, P. Madhavan, S. Vijayabalan, A. Chia, K. Fukui, *PeerJ* **2020**, *8*, e10003.

[60] M. Zhang, H. Zheng, Y. Gao, B. Zheng, J. Liu, H. Wang, Z. Yang, Z. Zhao, *J. Toxicol. Environ Health A* **2017**, *80*, 1199.
[61] J. H. Bae, J. M. Lee, B. G. Chung, *Biomed. Mater.* **2016**, *11*, 015019.
[62] G. Evin, A. Weidemann, *Peptides (N.Y.)* **2002**, *23*, 1285.
[63] E. Portelius, N. Bogdanovic, M. K. Gustavsson, I. Volkmann, G. Brinkmalm, H. Zetterberg, B. Winblad, K. Blennow, *Acta Neuropathol.* **2010**, *120*, 185.
[64] M.-N. Labour, S. Vigier, D. Lerner, A. Marcilhac, E. Belamie, *Acta Biomater.* **2016**, *37*, 38.
[65] Y. J. Choi, J. Park, S.-H. Lee, *Biomaterials* **2013**, *34*, 2938.
[66] W. E. Klunk, R. F. Jacob, R. P. Mason, *Methods Enzymol.* **1999**, *309*, 285.
[67] C. Wu, J. Scott, J. E. Shea, *Biophys. J.* **2012**, *103*, 550.
[68] R. A. Armstrong, *Folia Neuropathol.* **2007**, *45*, 108.
[69] A. S. Abdul Manap, A. C. Wei Tan, W. H. Leong, A. Y. Yin Chia, S. Vijayabalan, A. Arya, E. H. Wong, F. Rizwan, U. Bindal, S. Koshy, P. Madhavan, *Front Aging Neurosci.* **2019**, *11*, 206.
[70] H. Cai, Z. Ao, L. Hu, Y. Moon, Z. Wu, H.-C. Lu, J. Kim, F. Guo, *Analyst* **2020**, *145*, 6243.
[71] J. I. Forster, S. Köglsberger, C. Trefois, O. Boyd, A. S. Baumuratov, L. Buck, R. Balling, P. M. A. Antony, *J. Biomol. Screen* **2016**, *21*, 496.
[72] J. Krishtal, O. Bragina, K. Metsla, P. Palumaa, V. Tõugu, *PLoS One* **2017**, *12*, e0186636.
[73] D. M. Bowen, C. B. Smith, P. White, A. N. Davison, *Brain* **1976**, *99*, 459.
[74] G. K. Wilcock, M. M. Esiri, D. M. Bowen, C. C. T. Smith, *J. Neurol. Sci.* **1982**, *57*, 407.
[75] L. M. de Medeiros, M. A. De Bastiani, E. P. Rico, P. Schonhofen, B. Pfaffenseller, B. Wollenhaupt-Aguiar, L. Grun, F. Barbé-Tuana, E. R. Zimmer, M. A. A. Castro, R. B. Parsons, F. Klamt, *Mol. Neurobiol.* **2019**, *56*, 7355.
[76] F. J. Gil-Bea, M. García-Alloza, J. Domínguez, B. Marcos, M. J. Ramírez, *Neurosci. Lett.* **2005**, *375*, 37.
[77] S.-Y. Park, H.-S. Kim, E.-K. Cho, B.-Y. Kwon, S. Phark, K.-W. Hwang, D. Sul, *Food Chem. Toxicol.* **2008**, *46*, 2881.
[78] J. Yan, J. Hu, A. Liu, L. He, X. Li, H. Wei, *Bioorg. Med. Chem.* **2017**, *25*, 2946.
[79] Z. Feng, Y. Li, Y. Bai, *Vet Med. Sci.* **2021**, *7*, 1938.
[80] H. Park, J. Kim, C. Ryou, *Cell Prolif.* **2023**, *56*, e13399.
[81] D. Lee, S. M. Kim, H. Y. Kim, Y. Kim, *ACS Chem. Neurosci.* **2019**, *10*, 2647.
[82] H. Kim, B.-S. Park, K.-G. Lee, C. Y. Choi, S. S. Jang, Y.-H. Kim, S.-E. Lee, *J. Agric. Food Chem.* **2005**, *53*, 8537.
[83] R. Mallesh, J. Khan, P. K. Gharai, M. U. Arshi, S. Garg, S. Gupta, S. Ghosh, *ACS Chem. Neurosci.* **2024**, *15*, 2372.
[84] X. Ding, F. Liu, H. Wang, Y. Wang, G. Li, X. Zhang, C. Song, F. Zhu, D. Liu, *Brain Res.* **2024**, *1842*, 149102.
[85] H. S. Kundaikar, M. S. Degani, *Chem. Biol. Drug Des.* **2015**, *86*, 805.
[86] F. Yang, G. P. Lim, A. N. Begum, O. J. Ubeda, M. R. Simmons, S. S. Ambegaokar, P. P. Chen, R. Kayed, C. G. Glabe, S. A. Frautschy, G. M. Cole, *J. Biol. Chem.* **2005**, *280*, 5892.
[87] W. Yin, X. Zhang, Y. Li, *Neural Regen. Res.* **2012**, *7*.
[88] L. Zhang, Y. Fang, X. Cheng, Y. Lian, Z. Zeng, C. Wu, H. Zhu, H. Xu, *Biomed Res. Int.* **2018**, *2018*, 8134902.
[89] J. Kovalevich, D. Langford, *Methods Mol. Biol.* **2013**, *1078*, 9.
[90] Ö. Yildirim-Semerci, A. Arslan-Yildiz, *Microfluid Nanofluidics* **2024**, *28*, 42.
[91] R. Bilginer, D. Ozkendir-Inanc, U. H. Yildiz, A. Arslan-Yildiz, *J. Appl. Polym. Sci.* **2021**, *138*, 50287.
[92] O. Strada, S. Vyas, E. C. Hirsch, M. Ruberg, A. Brice, Y. Agid, F. Javoy-Agid, *Proc. Natl. Acad. Sci.* **1992**, *89*, 9549.
[93] A. S. Abdul Manap, A. C. Wei Tan, W. H. Leong, A. Y. Yin Chia, S. Vijayabalan, A. Arya, E. H. Wong, F. Rizwan, U. Bindal, S. Koshy, P. Madhavan, *Front. Aging Neurosci.* **2019**, *10*, 206.
[94] S. Sharma, H. Goyal, S. Joshi, B. Nehru, A. Saini, *Advances in Redox Research*, **2023**, *7*, 100060.